



**HAL**  
open science

## Effect of MO<sub>2</sub> (M = Ce, Mo, Ti) layer on activity and stability of PtCo/C catalysts during an oxygen reduction reaction

Napapat Chaisubanan, Mali Hunsom, Hugues Vergnes, Kejvalee Pruksathorn

► **To cite this version:**

Napapat Chaisubanan, Mali Hunsom, Hugues Vergnes, Kejvalee Pruksathorn. Effect of MO<sub>2</sub> (M = Ce, Mo, Ti) layer on activity and stability of PtCo/C catalysts during an oxygen reduction reaction. Energy Conversion and Management, 2016, 114, pp.348-355. 10.1016/j.enconman.2016.02.033 . hal-01912000

**HAL Id: hal-01912000**

**<https://hal.science/hal-01912000>**

Submitted on 5 Nov 2018

**HAL** is a multi-disciplinary open access archive for the deposit and dissemination of scientific research documents, whether they are published or not. The documents may come from teaching and research institutions in France or abroad, or from public or private research centers.

L'archive ouverte pluridisciplinaire **HAL**, est destinée au dépôt et à la diffusion de documents scientifiques de niveau recherche, publiés ou non, émanant des établissements d'enseignement et de recherche français ou étrangers, des laboratoires publics ou privés.



## Open Archive Toulouse Archive Ouverte (OATAO)

OATAO is an open access repository that collects the work of some Toulouse researchers and makes it freely available over the web where possible.

This is an author's version published in: <http://oatao.univ-toulouse.fr/20539>

**Official URL:** <https://doi.org/10.1016/j.enconman.2016.02.033>

### **To cite this version:**

Chaisubanan, Napapat and Hunsom, Mali and Vergnes, Hugues and Pruksathorn, Kejvalee Effect of MO<sub>2</sub> (M = Ce, Mo, Ti) layer on activity and stability of PtCo/C catalysts during an oxygen reduction reaction. (2016) Energy Conversion and Management, 114. 348-355. ISSN 0196-8904

Any correspondance concerning this service should be sent to the repository administrator:  
[tech-oatao@listes-diff.inp-toulouse.fr](mailto:tech-oatao@listes-diff.inp-toulouse.fr)

# Effect of MO<sub>2</sub> (M = Ce, Mo, Ti) layer on activity and stability of PtCo/C catalysts during an oxygen reduction reaction

Napapat Chaisubanan<sup>a</sup>, Mali Hunsom<sup>a,b</sup>, Hugues Vergnes<sup>c</sup>, Kejvalee Pruksathorn<sup>a,b,\*</sup>

<sup>a</sup>Fuels Research Center, Department of Chemical Technology, Faculty of Science, Chulalongkorn University, 254 Phayathai Road, Bangkok 10330, Thailand

<sup>b</sup>Center of Excellence on Petrochemical and Materials Technology (PETRO-MAT), Chulalongkorn University, 254 Phayathai Road, Bangkok 10330, Thailand

<sup>c</sup>Laboratoire de Génie Chimique, ENSIACET, Institut National Polytechnique de Toulouse, UMR-CNRS 5503, 4 allée Emile Monso, 31030 Toulouse Cedex 4, France

## A B S T R A C T

The performance of PtCo/C catalysts in the presence of a metal oxides layer for an oxygen reduction reaction (ORR) was investigated. Different types of metal oxides (CeO<sub>2</sub>, MoO<sub>2</sub> and TiO<sub>2</sub>) and metal loadings (0.03–0.45 mg/cm<sup>2</sup>) were incorporated on the PtCo/C catalyst layer. Their activity was analyzed in acid solution and proton exchange membrane (PEM) fuel cell under a H<sub>2</sub>/O<sub>2</sub> environment at 60 °C and ambient pressure, while the stability was tested in an N<sub>2</sub>-saturated H<sub>2</sub>SO<sub>4</sub> solution using repetitive potential cycling. It was found that the addition of metal oxides on a catalyst layer had no influence for PtCo/C morphology. However, they significantly affected the electrochemical surface area (ESA), internal contact resistance (ICR) and hydrophilic/hydrophobic properties of the catalysts layer. Furthermore, they significantly affected the ORR activity and stability in acid solution and PEM fuel cell operation. Among all studied metal oxides, the TiO<sub>2</sub> exhibited the best property for use as the catalyst interlayer in PEM fuel cell for both activity and stability enhancement.

## Keywords:

PtCo/C catalyst  
PEM fuel cell  
Metal oxide  
Titanium dioxide

## 1. Introduction

The PEM fuel cell is an electrochemical apparatus that produces electricity effectively and continuously in the presence of continuous reactant feed with zero emission of contaminants [1]. To facilitate the utilization and commercialization of PEM fuel cells, their cost and reliability/durability have to be addressed. Their major cost can be attributed to the utilization of an expensive Pt metal as the catalyst in the electrode layer [2]. Thus, many researchers have been developed the new types of fuel cell catalysts such as non-Pt catalysts [1,3–8], Pt-based catalysts [9–12] and non-precious metal composite electrocatalysts [13–15] as a means to reduce fuel cell cost. Among these, the most promising catalysts are the nanostructured Pt-alloy catalysts because they can enhance activity levels to a high degree when compared with pure Pt catalysts [16]. The Pt–Co alloy catalyst is the most interest because it showed the highest fuel cell performance and more stable than other Pt–M alloys (M = V, Ni, Fe) [17,18]. The loss of fuel cell durability is principally caused by the loss of fuel cell components: catalyst, membrane or bipolar plate [19], which can be alleviated by

using appropriate material to fabricate a fuel cell or appropriate operating conditions. Another strategy that can extend the lifetime and activity of fuel cells is the water management strategy [20]. This is because accumulation of excessive water in fuel cells leads to flooding, which causes low accessibility of reactant to the reaction zone, particularly at high current. However, too low water in fuel cells results in dry out of the membrane, which causes sluggishness of proton transfer to the membrane as well as damage of cell components. Thus, various water management strategies have been developed to optimize water content in a fuel cell, particularly in the catalyst layer. The addition of a conductive material plate with perforations between the flow field plate and electrocatalyst substrate can enhance the operational life of a PEM fuel cell for no humid conditions [21]. This then leads to improvement of water management in fuel cells. The mesoporous hydrophobic channels, made as a tubular open-ended mesopores through the catalysts with addition of PTFE nanoparticles, can reduce the concentration loss at high current of the PEM fuel cell owing to its capability for water removal [20]. The incorporation of a double-layer cathode gas diffusion media (GDM) with high PTFE content in the fuel cell can improve the ability of water management as it can reduce the overall saturation level and voltage fluctuations [22]. The addition of a GDL coated with hydrophilic carbon in microporous layer exhibited an ability to conserve membrane humidity under low humidity conditions due to its ability to expel

\* Corresponding author at: Fuels Research Center, Department of Chemical Technology, Faculty of Science, Chulalongkorn University, 254 Phayathai Road, Bangkok 10330, Thailand. Tel.: +66 (2) 2187523; fax: +66 (2) 2555831.

E-mail address: [kejvalee.p@chula.ac.th](mailto:kejvalee.p@chula.ac.th) (K. Pruksathorn).

## Nomenclature

$j_k$	kinetic current density (mA/cm <sup>2</sup> )	$D$	diffusion coefficient of oxygen in solution (1.9 × 10 <sup>-5</sup> cm <sup>2</sup> /s)
$j$	current density (mA/cm <sup>2</sup> )	$\nu$	kinematics viscosity (0.01 cm <sup>2</sup> /s)
$\omega$	rotation rate (rpm)	$C$	oxygen concentration in the bulk solution (1.1 × 10 <sup>-6</sup> mol/cm <sup>3</sup> )
$n_e$	number of involved electrons		
$F$	Faraday's constant (96,485 C/mol)		

water and maintain oxygen on electrocatalyst electrode [23]. In previous work of Chaisubanan et al. [24], the PtCo/C catalyst with TiO<sub>2</sub> in mixed phase of anatase and rutile could improve the hydrophilic property of PtCo/C catalyst layer and had significant effect on the PEM fuel cell performance in middle to high voltage than that of PtCo/C catalyst with TiO<sub>2</sub> in rutile phase.

In the present study, the various types and loadings of the MO<sub>2</sub>/PtCo/C catalyst (M = Ce, Mo, Ti) were investigated to determine their effect on water management in the PEM fuel cell. The ORR activity and stability of all prepared catalysts were also explored. This is because they have different hydrophilic/hydrophobic properties and, as mentioned previously, the interface of Pt and metal oxide are the ORR active sites [25]. It was then expected that these properties of metal oxides would facilitate a high ORR activity as truly as the stability of PEM fuel cell.

## 2. Experimental

### 2.1. Preparation of catalyst-coated membrane

The PtCo/C catalyst was produced by H<sub>2</sub>PtCl<sub>6</sub>·6H<sub>2</sub>O (Sigma-Aldrich) and CoCl<sub>2</sub>·6H<sub>2</sub>O (Kanto Chemical) as the precursors and NaBH<sub>4</sub> (Labchem) as the reducing agent. The method of the preparation was same as research of Chaisubanan et al. [24] as shown in Fig. 1.

To prepare the catalyst-coated membrane, the mixture of PtCo/C catalyst and distilled H<sub>2</sub>O was sonicated at approximate 30 °C for 30 min. Sequentially, Nafion solution (5 wt%, Fluka) and *i*-propanol (99.99%, Fisher) were added and sonicated for 1 h to obtain catalyst ink with a catalyst to Nafion weight ratio of 67:33 [26]. Afterward,

the ink was sprayed slowly onto the Nafion membrane 115 at 80 °C by a spray gun (Crescendo, Model 175-7™) and left at room temperature to dry the catalyst layer for a few minute. This method was repeated to obtain a metal of 0.15 mg/cm<sup>2</sup> and dried at the same temperature for 10 min. For an anode side, the commercial 20 wt% Pt/C (E-TEK) was applied by the same method at identical Nafion content and catalyst loading (0.15 mg/cm<sup>2</sup>).

### 2.2. Preparation of metal oxide-coated PtCo/C catalyst

Three types of commercial metal oxides, including TiO<sub>2</sub> (P25 Degussa, Sigma-Aldrich), MoO<sub>2</sub> (Sigma-Aldrich) and the as-prepared CeO<sub>2</sub>, prepared by the calcination of Ce(NO<sub>3</sub>)<sub>3</sub>·6H<sub>2</sub>O (Sigma-Aldrich) at 600 °C for 90 min [27] were used in this study. To incorporate commercial TiO<sub>2</sub> and CeO<sub>2</sub> on the catalyst layer at different loadings of 0.03, 0.06, 0.15, 0.30 and 0.45 mg/cm<sup>2</sup>, 0.4, 0.8, 1.5, 3.0 and 5.0 mg of either TiO<sub>2</sub> or CeO<sub>2</sub> were mixed with 6 mL of *i*-propanol and sonicated 15 min at ambient temperature. For MoO<sub>2</sub>, a similar quantity of MoO<sub>2</sub> as TiO<sub>2</sub> and CeO<sub>2</sub> were dispersed in 6 mL of ethanol (Merck) and resonicated for 30–60 min. Sequentially, the metal oxide slurry was applied on the PtCo/C catalyst layer by direct spray. Finally, the ready-to-use metal oxide-coated PtCo/C catalyst (MO<sub>2</sub>/PtCo/C) was obtained after drying at 80 °C for 30 min.

### 2.3. Preparation of membrane electrode assembly (MEA)

The MEA was fabricated by a conventional process, and described in Chaisubanan et al. [24]. In brief, the sublayer ink-coated GDL was formulated by mixing of deionized water, 60%

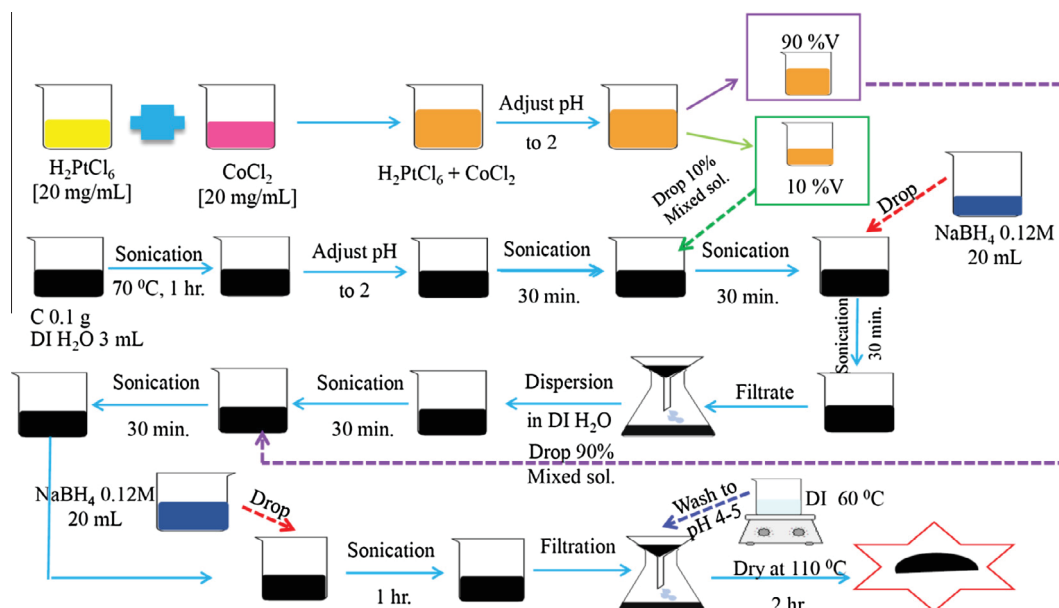


Fig. 1. Schematic representation of 30 wt% PtCo/C catalyst preparation by the seeding and impregnation method.

(w/w) polytetrafluoroethylene, *i*-propanol and treated carbon in ultrasonic bath at the ambient temperature for 30 min. The ink was brushed on a GDL (carbon cloth, ETEK) several times to get the loading of carbon of  $\sim 2.0$  mg/cm<sup>2</sup>. After that, it was dried 1 h at 300 °C to remove an excess solvent. Afterward, the catalyst coated membrane (Section 2.1) was pressed between coated GDL sheets by a compression mold at 65 kg/cm<sup>2</sup> and 137 °C for 2.5 min and cool pressed at ambient temperature for 2.5 min.

#### 2.4. ORR activity test

The ORR activities of all catalysts were tested by a rotating disk electrode (RDE) in H<sub>2</sub>SO<sub>4</sub> solution saturated with oxygen and in the PEM fuel cell with H<sub>2</sub>/O<sub>2</sub> environment. The other test was carried out in the fuel cell environment by mounting the MEA obtained from Section 2.3 on commercial hardware and testing in a test station at 60 °C and ambient pressure. The 100 sccm of humidified H<sub>2</sub> and O<sub>2</sub> were fed into the anode and cathode, respectively. Prior to drawing the current, the cell was run at high current density ( $>700$  mA/cm<sup>2</sup>) for a certain period. Subsequently, the current was drawn between the open circuit potential (OCP) to 0.1 V and demonstrated in terms of a performance curve or current-density-potential curves. For the activity test in H<sub>2</sub>SO<sub>4</sub> solution, the catalyst ink prepared was coated on the circular GDL with 1 cm diameter, assembled with the RDE using as a working electrode. A Pt gauze and the saturated calomel electrode (SCE) were used as the counter and reference electrodes respectively. The 0.5 M H<sub>2</sub>SO<sub>4</sub> was bubbled by O<sub>2</sub> gas for 1–2 h before the test. The ORR activity of the MO<sub>2</sub>/PtCo/C catalyst was determined by linear sweep voltammetry (LSV) under a GPES program connected with the Potentiostat/Galvanostat, at 25 °C and atmospheric pressure. The studied potential range was  $-0.05$  to  $0.65$  V at varying rotation rates (500–2000 rpm) and 10 mV/s sweep rate.

#### 2.5. Catalyst or electrode characterizations

The structure of all catalysts was characterized by X-ray diffraction (XRD, D8 Discover-Bruker AXS). The morphology and metal dispersion were characterized by the scanning electron microscopy (SEM) with energy dispersive X-ray spectroscopy (EDX) on a JSM 6400 machine. The ICR of MO<sub>2</sub>/PtCo/C catalysts was tested by a homemade through-plane test system. The  $1.0 \times 1.5$  cm of MO<sub>2</sub>/PtCo/C catalyst coated electrodes were cut and placed between the two copper test electrodes. The current was applied in the range of 0.01–0.2 A by a DC power supply (Mastech, HY3002), and the voltage was measured by a voltmeter (Richtmass, RM-15). The conductivity of MO<sub>2</sub>/PtCo/C catalysts was measured at 25 °C by 4-probe apparatus (Jandel, RM3-AR). The water contact angle of all catalysts was evaluated by the Standard Contact Angle Goniometer (Rame'hart, 200-U1). The ESA was estimated from the H<sub>2</sub> stripping method in H<sub>2</sub>SO<sub>4</sub> solution

saturated with N<sub>2</sub> with the potential range of  $-0.24$  to  $+1.00$ V and 20 mV/s of scan rate by potentiostat/galvanostat (DEA332, Radiometer) [28]. A Pt gauze and the saturated calomel electrode (SCE) were used as the counter and reference electrodes respectively. The corrosion of all MO<sub>2</sub>/PtCo/C catalysts was tested in 0.5 M H<sub>2</sub>SO<sub>4</sub> in the potential range of  $-0.58$  to  $0.02$  V with scan rate of 1 mV/s using the LSV program connected with the Potentiostat/Galvanostat (PGSTAT 30, Autolab). The as-prepared catalysts were used as working electrode, a Pt gauze was used as counter electrode and saturated calomel electrode (SCE) was used as reference electrode.

In this work, all experimental data were obtained from 3 experiments with the accepted error of less than 3%.

### 3. Results and discussion

#### 3.1. Physical and chemical characterizations of metal oxides (MO<sub>2</sub>) and MO<sub>2</sub>/PtCo/C catalysts

The SEM images of all metal oxides used in this work are demonstrated in Fig. 2. At identical magnification, both CeO<sub>2</sub> and MoO<sub>2</sub> demonstrated their structure as a large flat sheet. A smoother surface was observed for MoO<sub>2</sub> than for CeO<sub>2</sub>, probably because the former metal oxide had a higher crystallinity than that of the latter metal oxide. The TiO<sub>2</sub> demonstrated an almost spherical shape with a smaller particle size than other metal oxides. Regarding their crystal structures, the XRD pattern of CeO<sub>2</sub> demonstrated peaks at 28.59°, 33.03°, 47.31° and 56.03°, assigned to [111], [200], [220] and [311] crystalline planes, respectively, indicating a face-centered cubic of CeO<sub>2</sub> (Fig. 3). Sharp XRD peaks were observed for MoO<sub>2</sub> at 26.1°, 37.1°, 53.6° and 60.1°, corresponding respectively to the [011], [211], [022] and [031] lattice planes of the monoclinic MoO<sub>2</sub> crystal, suggesting a greater crystallinity than that of CeO<sub>2</sub>. The XRD peaks of TiO<sub>2</sub> demonstrated the main characteristic peaks of a mixed phase of the anatase phase (A) at a  $2\theta$  of 25.65°, 37.60°, 48.38°, 54.23°, and 55.65° and the rutile phase (R) at a  $2\theta$  of 27.51° and 62.26°, corresponding to the A[101], A[004], A[200], A[105], A[211], R[110], and R[002] planes, respectively. The particle sizes, calculated by the Scherrer equation, of CeO<sub>2</sub>, MoO<sub>2</sub> and TiO<sub>2</sub> were 44.21, 41.61, and 11.59 nm, respectively.

When all metal oxides were incorporated on PtCo/C catalyst surface, they distributed uniformly along the catalyst surface (Fig. 4) and had an insignificant effect on either crystalline size or *d*-spacing of the catalysts as well as the weight ratio of Pt:Co (1:1). The crystalline size or *d*-spacing of the PtCo/C and MO<sub>2</sub>/PtCo/C catalysts were still between 0.222–0.225 nm and 7.41–7.67 nm, respectively (Data not shown).

The ESA was then determined from the H<sub>2</sub> desorption peak, obtained from the CV experiment carried out in the potentials range of  $-0.35$  to  $1.2$  V/SCE, 20 mV/s scan rate under N<sub>2</sub>

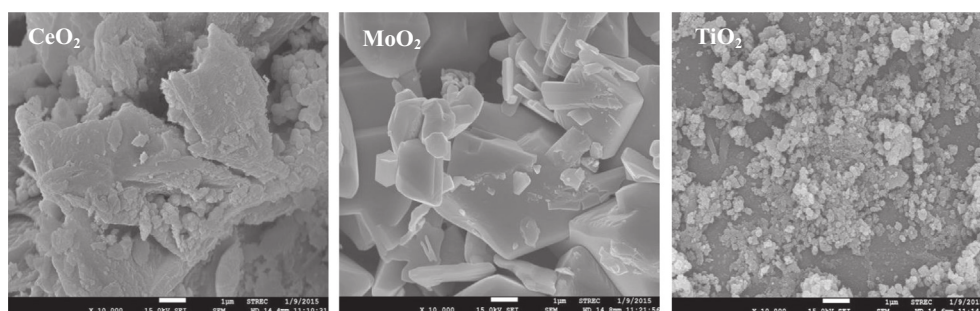


Fig. 2. SEM images of commercial metal oxides at 10,000 $\times$  magnification.

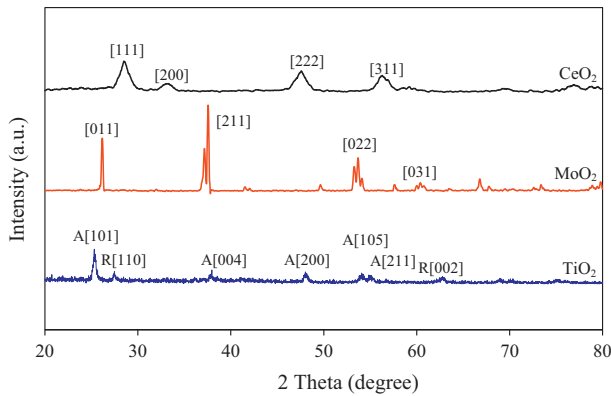


Fig. 3. XRD pattern of all utilized commercial metal oxides.

atmosphere. As demonstrated in Fig. 5, the presence of  $\text{CeO}_2$  affected negatively the ESA of the PtCo/C catalyst. Namely, the ESA was reduced almost 50% in the presence of  $\text{CeO}_2$  at all investigated loadings in the range of 0.03–0.45  $\text{mg}/\text{cm}^2$ . In addition, the presence of  $\text{MoO}_2$  at any loadings in the range of 0.03–0.45  $\text{mg}/\text{cm}^2$  affected negatively the PtCo/C catalyst ESA. More amount of  $\text{MoO}_2$  loading led to the decreasing catalyst ESA. The decreasing

ESA with increasing  $\text{CeO}_2$  and  $\text{MoO}_2$  loading is probably attributed to their large particle size compared with that of the PtCo/C, which could decrease an available Pt active site to precede the reaction. Interestingly, the addition of  $\text{TiO}_2$  on the layer of PtCo/C catalysts gave both positive and negative influences on their ESA. Increasing the  $\text{TiO}_2$  from 0.03 to 0.06  $\text{mg}/\text{cm}^2$  gave an increasing ESA. Then, greater than 0.15  $\text{mg}/\text{cm}^2$  of  $\text{TiO}_2$  content led to decreasing ESA. The augmentation of ESA at low  $\text{TiO}_2$  content could be involved to the growth of electrode roughness. However, over content of  $\text{TiO}_2$ , especially more than 0.30  $\text{mg}/\text{cm}^2$ , might induce the blockage of active catalyst surface as well as the disconnection of the electron-conducting network through the catalyst layer, resulting of a decreasing ESA.

With regard to the effect of metal oxides on the conductivity of the catalyst, the result showed that the incorporation of metal oxides at all loadings in the range of 0.03–0.45  $\text{mg}/\text{cm}^2$  led to an increase of ICR of catalyst layer (Fig. 6). In other words, the conductivity of catalyst decreased with the increase of metal oxide loading. This is because the oxygen molecule on the metal oxide structure can reduce the electron mobility along a carbon surface and other elements [29]. Among all  $\text{MO}_2/\text{PtCo}/\text{C}$  catalysts, the  $\text{TiO}_2/\text{PtCo}/\text{C}$  catalyst exhibited the lowest ICR, probably due to the fact that  $\text{TiO}_2$  can form a more percolating electron-conducting network in the catalyst layer than that of  $\text{CeO}_2$  and

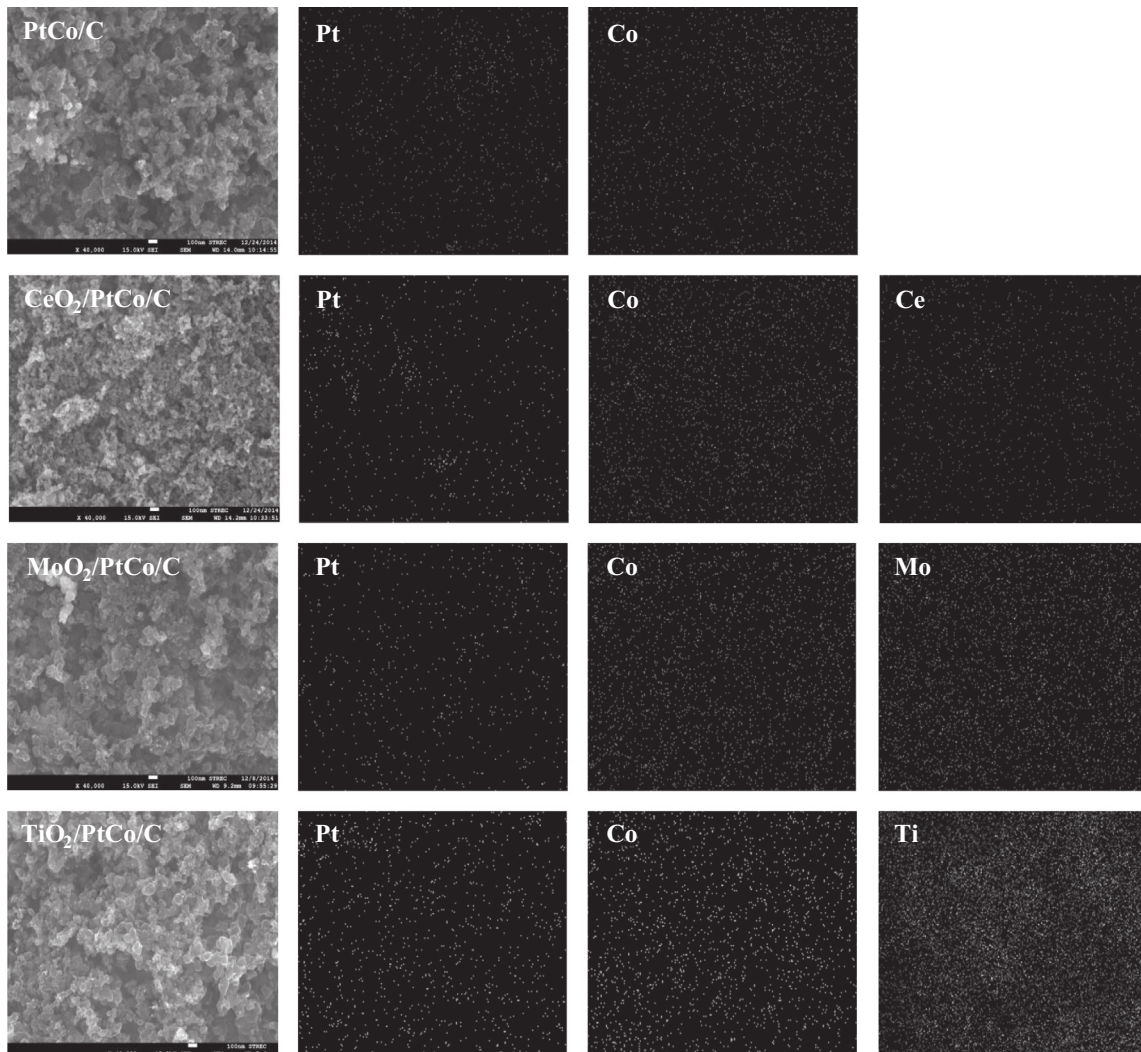


Fig. 4. SEM image and mapping of metal element obtained from the EDX measurement on PtCo/C catalysts with different metal oxides.

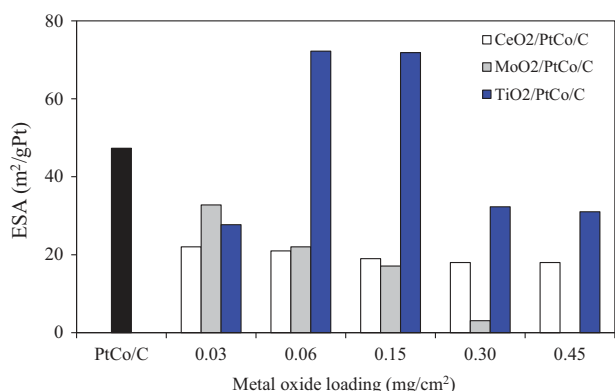


Fig. 5. ESA of PtCo/C catalysts with and without metal oxides loading.

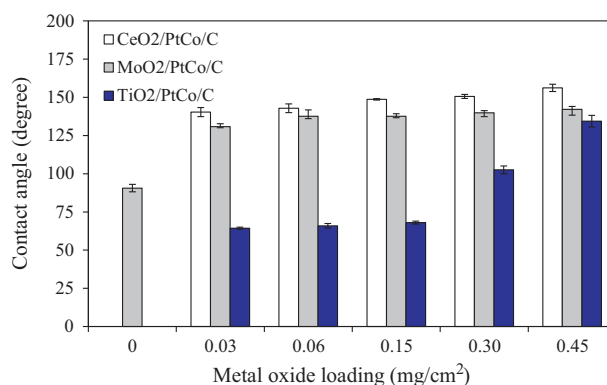


Fig. 7. Contact angle of PtCo/C catalysts with and without of metal oxides loading.

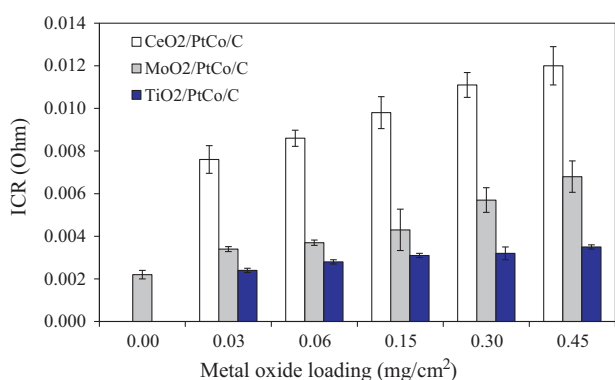


Fig. 6. Internal contact resistance (ICR) of PtCo/C catalysts with and without metal oxides loading.

MoO<sub>2</sub>. The conductivity of CeO<sub>2</sub>, MoO<sub>2</sub> and TiO<sub>2</sub> were measured at 25 °C as 0.071, 0.167, and 9.432 S/m, respectively.

The influence of MO<sub>2</sub> on the hydrophilic/hydrophobic properties of the PtCo/C catalyst was then analyzed in terms of water contact angle. Theoretically, the material having a contact angle greater than 150° exhibits the superhydrophobic property, while the material having a contact angle between 65° and 150° demonstrates the hydrophobic property. The hydrophilic material usually has a contact angle between 0° and 65°, and the superhydrophilic material exhibits a contact angle of around 0° [30]. As demonstrated in Fig. 7, the original PtCo/C catalyst had a contact angle of 90.6°, exhibiting the hydrophobic property. The incorporation of both CeO<sub>2</sub> and MoO<sub>2</sub> on the PtCo/C catalyst layer induced an increase of the contact angle of such a catalyst, suggesting an increase of hydrophobic properties of the PtCo/C catalyst. Increasing the CeO<sub>2</sub> and MoO<sub>2</sub> loading in the catalyst surface led to an increase of hydrophobic properties of the catalyst. For the TiO<sub>2</sub>/PtCo/C catalyst, it exhibited the hydrophilic property at low TiO<sub>2</sub> loading (0.03–0.15 mg/cm<sup>2</sup>) and hydrophobic property at high TiO<sub>2</sub> loading (0.30–0.45 mg/cm<sup>2</sup>). Theoretically, the TiO<sub>2</sub> has the hydrophilic properties [31]. Thus, the PtCo/C catalyst exhibited the hydrophilic property at low TiO<sub>2</sub> content. However, in the presence of high TiO<sub>2</sub> content, the PtCo/C catalyst exhibited the hydrophobic property; this is probably due to the effect of its high roughness. As mentioned previously, the hydrophobic property of TiO<sub>2</sub> increases as the increase of TiO<sub>2</sub> layer roughness [32,33], which is usually found in the presence of thick TiO<sub>2</sub> layer. In this work, different loadings of TiO<sub>2</sub> were loaded on identical area of catalyst layer, thus the thickness of TiO<sub>2</sub> increased as the increase of TiO<sub>2</sub>, which is consequently induced an increase of surface roughness as well as the hydrophobic property of catalyst layer.

### 3.2. ORR activity of MO<sub>2</sub>/PtCo/C catalysts

The ORR activity of MO<sub>2</sub>/PtCo/C catalysts was first analyzed in H<sub>2</sub>SO<sub>4</sub> solution saturated by oxygen. The operating condition was at RDE rates of 500–2000 rpm, potential range of –0.05 to 0.65 V and 10 mV/s of scan rate. Fig. 8(a) showed the same pattern of the current density–potential curve for all MO<sub>2</sub>/PtCo/C catalysts. From this pattern, it can be explained in three parts as kinetic control region, mixed control region and mass transfer region. The first region was observed during the potential of 0.65–0.45 V where mass transfer and rotation ( $\omega$ ) rates had not affect the current density. The second region appeared at 0.45–0.30 V. The current was uncompletely controlled by electron and mass transfers. The current increased with increasing of rotating rate in nonlinear function of square root of rotation rate ( $\omega^{1/2}$ ). The last region

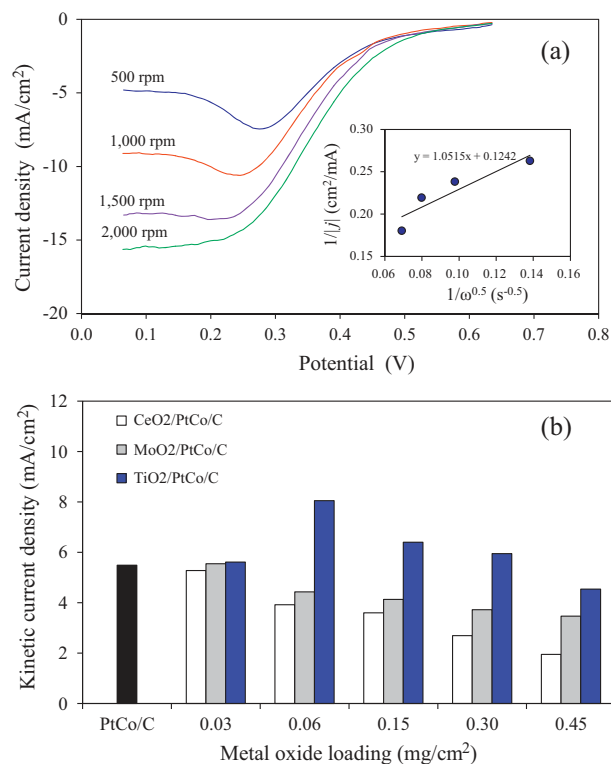


Fig. 8. (a) Voltammogram for the ORR of TiO<sub>2</sub>/PtCo/C catalyst (at loading of 0.06 mg/cm<sup>2</sup>) and (b) kinetic current of MO<sub>2</sub>/PtCo/C catalysts at different metal oxide loadings in H<sub>2</sub>SO<sub>4</sub> solution saturated with O<sub>2</sub> at 0.385 V with 10 mV/s of scan rate.

appeared at 0.3–0.05 V, showed a plateau of limiting current that increased linearly with square root of rotation rate ( $\omega^{1/2}$ ) [24].

The current density was as a first order function of the rotating rate expressing by the Koutecky–Levich equation, which is valid for the diffusion species as demonstrated by [34]:

$$\frac{1}{j} = \frac{1}{j_k} + \frac{1}{B\omega^{1/2}} \quad (1)$$

and where  $B$  is determined by Eq. (2),

$$B = 0.62n_eFD^{2/3}v^{-1/6}C \quad (2)$$

The function of  $j^{-1}$  vs.  $\omega^{-1/2}$  at particular potentials (the insert of Fig. 8(a)) provided straight lines, allowing the calculation of the kinetic current density ( $j_k$ ) from intercept and number of electrons involved in the ORR reaction from slope. The summary of kinetic plot of all  $\text{MO}_2/\text{PtCo}/\text{C}$  catalysts at different metal oxide loadings is shown in Fig. 8(b). The kinetic current density, or  $j_k$ , was found to depend on the loading of metal oxide.

The  $\text{MO}_2/\text{PtCo}/\text{C}$  catalysts in the presence of either  $\text{CeO}_2$  or  $\text{MoO}_2$  at all loadings in the range of 0.03–0.45  $\text{mg}/\text{cm}^2$  exhibited ORR activity less than that of the  $\text{PtCo}/\text{C}$  catalysts, probably because of their low ESA, high ICR as well as their hydrophobic property. The presence of  $\text{TiO}_2$  at appropriate loading (0.06  $\text{mg}/\text{cm}^2$ ) can promote an increase of ORR activity of the  $\text{PtCo}/\text{C}$  catalyst, which might be attributed to their high ESA, low ICR and appropriate hydrophobic/hydrophilic properties.

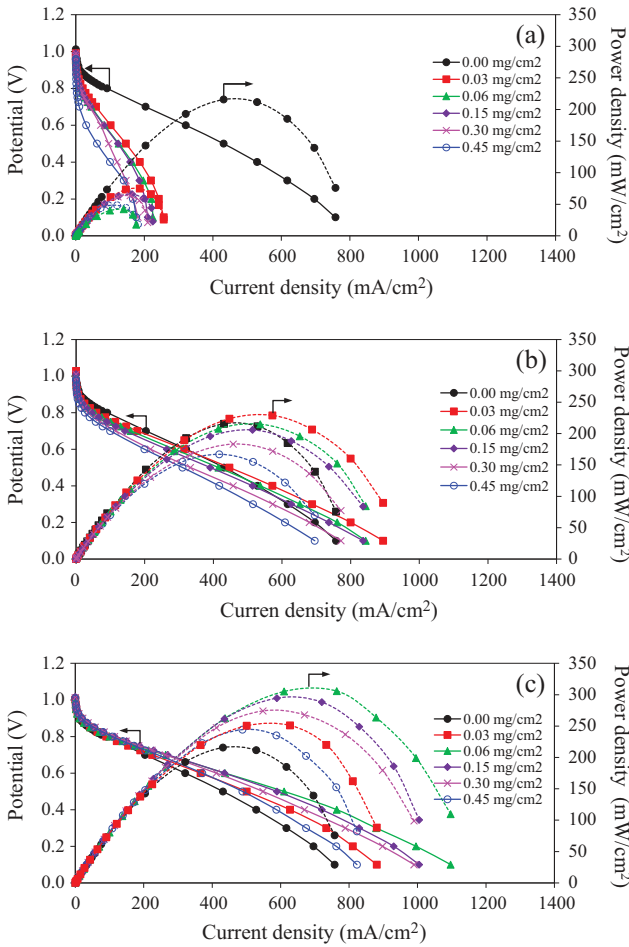


**Fig. 9.** Polarization curve of  $\text{PtCo}/\text{C}$  catalyst with different loadings of (a)  $\text{CeO}_2$  (b)  $\text{MoO}_2$  and (c)  $\text{TiO}_2$  in PEM fuel cell under  $\text{H}_2/\text{O}_2$  environment at 60 °C and ambient pressure.

To obtain the actual ORR activity of all prepared catalysts, all catalysts were analyzed in a PEM fuel cell using  $\text{H}_2/\text{O}_2$  gases at 60 °C at atmospheric pressure. The inclusion of  $\text{MO}_2$  in the  $\text{PtCo}/\text{C}$  catalyst layer affected insignificantly the OCP (Fig. 9). The presence of  $\text{CeO}_2$  or  $\text{MoO}_2$  affected negatively the performance of the  $\text{PtCo}/\text{C}$  catalyst at low current density, which could be ascribed to their low active surface area. The addition of  $\text{TiO}_2$  onto the  $\text{PtCo}/\text{C}$  catalyst surface had not affect the performance of the catalyst under this region. The performance loss of the  $\text{MO}_2/\text{PtCo}/\text{C}$  catalyst was more pronounced at ohmic region, which was initiated by the sluggishness of electron transfer through the electrodes and the sluggishness of protons ( $\text{H}^+$ ) flowing through the membrane. The addition of  $\text{CeO}_2$  and  $\text{MoO}_2$  at all loadings influenced negatively the current density at 0.6 V as displayed in Fig. 10, due to their high ICR as well as their hydrophobic property of the catalyst layer. From the plot, the water contact angles of  $\text{CeO}_2/\text{PtCo}/\text{C}$  and  $\text{MoO}_2/\text{PtCo}/\text{C}$  were close to 150°, indicating extremely high hydrophobicity of the catalyst layer, and their hydrophobicity increased with the increase of  $\text{CeO}_2$  and  $\text{MoO}_2$  loading. This behavior caused the rapid water removal from the catalyst layer and membrane, resulting in the loss of proton conductivity, which consequently deteriorated the cell performance.

For the  $\text{TiO}_2/\text{PtCo}/\text{C}$  catalyst, incorporation of  $\text{TiO}_2$  at low loading between 0.03 and 0.06  $\text{mg}/\text{cm}^2$  induced an increase of current at 0.6 V of the fuel cell. This is because low  $\text{TiO}_2$  content can ameliorate the hydrophilic property of the catalyst electrode to obstruct its fast dry out, which is confirmed obviously by their

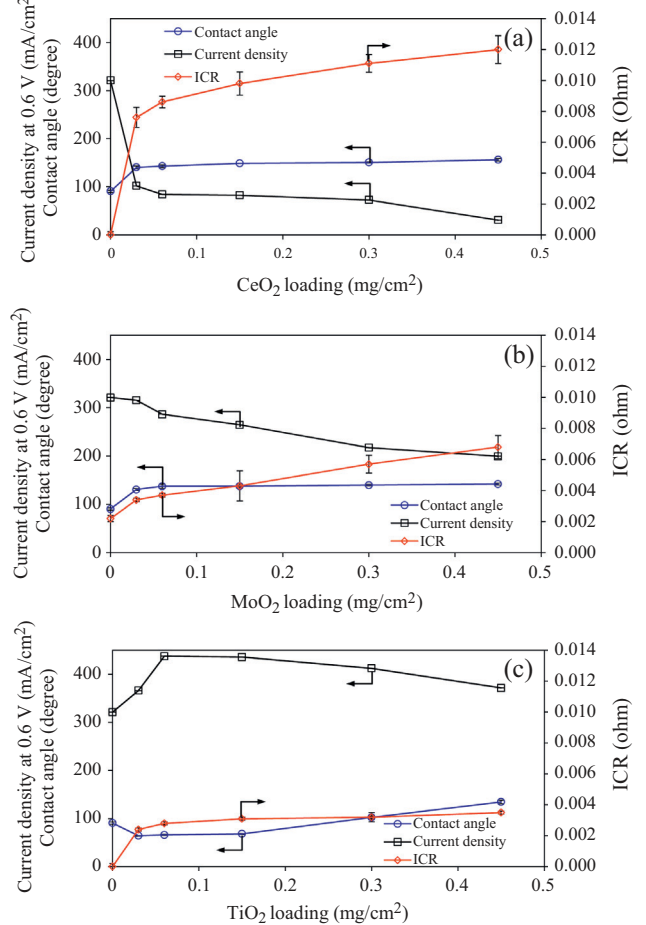


**Fig. 10.** Current density at 0.6 V, contact angle and ICR of  $\text{PtCo}/\text{C}$  catalyst with different loadings of (a)  $\text{CeO}_2$  (b)  $\text{MoO}_2$  and (c)  $\text{TiO}_2$ .

low value of water contact angle. Otherwise, the loading of  $\text{TiO}_2$  greater than  $0.15 \text{ mg/cm}^2$  induced a significant decreased fuel cell performance, probably due to a high mass transport limitation. Namely, an excess amount of  $\text{TiO}_2$  particles could adsorb an enormous quantity of water and consequently block the fuel/oxidant to react at catalyst site. One more possible reason, oxygen molecules could be adsorbed by  $\text{TiO}_2$ . It could capture electrons and donor  $\text{O}_2^-$  and also decrease dark conductivity [35,36]. So, the electrical conductivity was reduced 1.09- to 1.59-fold by the presence of 0.03–0.45  $\text{mg/cm}^2$   $\text{TiO}_2$  on PtCo/C catalyst. The cell performances were 1.14- to 1.36-fold more than that of the PtCo/C catalyst at 0.6 V. This is an effect of the hydrophilic property of  $\text{TiO}_2$  [24].

### 3.3. Stability of $\text{MO}_2/\text{PtCo/C}$ catalyst

The stability of all  $\text{MO}_2/\text{PtCo/C}$  catalysts was finally monitored by the change of ESA during the repetitive potential cycling experiment of these catalysts in  $\text{N}_2$ -saturated 0.5 M  $\text{H}_2\text{SO}_4$ . The example cyclic voltammogram of  $\text{MO}_2/\text{PtCo/C}$  catalysts was exhibits in Fig. 11(a). The similar pattern of cyclic voltammogram of all as-prepared catalyst was observed. Namely, the  $\text{H}_2$  adsorption peak appeared as a broad shoulder, not in a sharp peak, probably due to the partial overlapping with the oxygen atom reduction peaks (Pt–O reduction). The  $\text{H}_2$  desorption peak appeared as a clear sharp peak. Increasing the potential cycling to the 10th cycle resulted in the increase of peak intensity because of the humid Nafion membrane coating the catalyst [37]. Further increasing the repetitive potential cycling led to the decrease of peak intensity, indicating the decrease of ESA of the catalyst. As summarized in Fig. 11(b), the loss of normalized ESA of catalysts after 200 cycles was observed as the order of  $\text{CeO}_2/\text{PtCo/C} > \text{MoO}_2/\text{PtCo/C} > \text{PtCo/C} > \text{TiO}_2/\text{PtCo/C}$ . Approximately 78%, 43%, 28% and 20% were observed for  $\text{CeO}_2/\text{PtCo/C}$ ,  $\text{MoO}_2/\text{PtCo/C}$ , PtCo/C and  $\text{TiO}_2/\text{PtCo/C}$ , respectively. This suggests that the  $\text{TiO}_2/\text{PtCo/C}$  catalyst had the most stability compared with the other catalysts. This is probably due

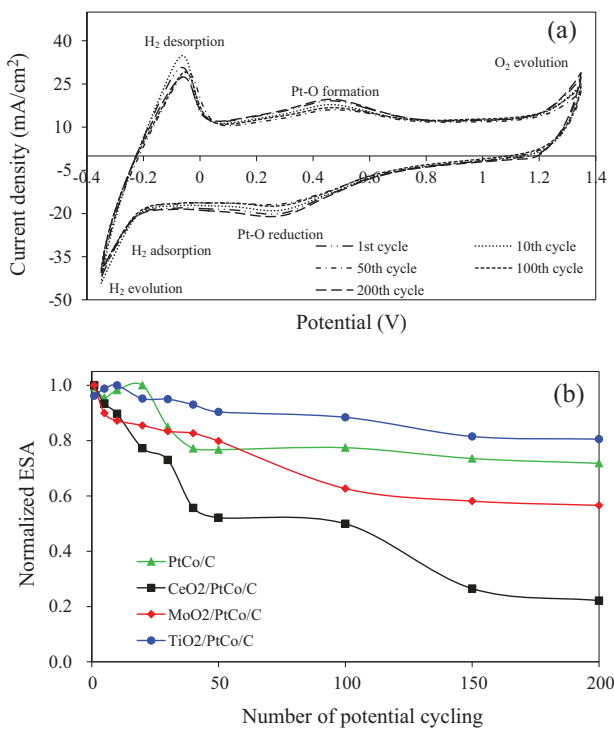


**Fig. 11.** (a) Cyclic voltammogram of  $\text{TiO}_2/\text{PtCo/C}$  catalyst versus numbers of repeated potential cycling in  $\text{H}_2\text{SO}_4$  solution at 20 mV/s of scan rate and (b) variation of normalized ESA.

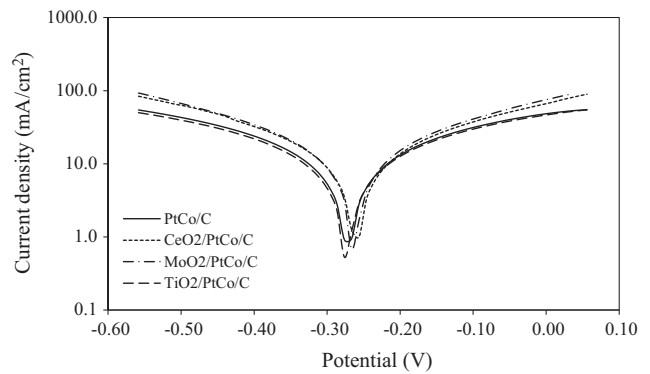


**Fig. 12.** Potentiodynamic polarization for corrosion of PtCo/C and  $\text{MO}_2/\text{PtCo/C}$  catalysts in 0.5 M  $\text{H}_2\text{SO}_4$  with the scan rate of 1 mV/s.

to a strong resistance of  $\text{TiO}_2$  in acid media. According to the results of corrosion test as demonstrated in Fig. 12, the magnitude of corrosion current density was changed as the order of  $\text{CeO}_2/\text{PtCo/C} > \text{MoO}_2/\text{PtCo/C} > \text{PtCo/C} > \text{TiO}_2/\text{PtCo/C}$  as 14.17, 9.37, 6.71 and 5.68  $\text{mA/cm}^2$ , respectively. This confirms that the  $\text{TiO}_2/\text{PtCo/C}$  exhibited the highest corrosion resistance compared to other  $\text{MO}_2/\text{PtCo/C}$  catalysts.

## 4. Conclusion

Three types of metal oxides, including  $\text{CeO}_2$ ,  $\text{MoO}_2$  and  $\text{TiO}_2$ , were incorporated as the interlayer of PtCo/C catalysts at different loadings. The results demonstrated that incorporation of those metal oxides had insignificant effect on either crystalline size or  $d$ -spacing of the PtCo/C catalyst. However, they have a significant effect on the ESA and ICR. Addition of  $\text{CeO}_2$  and  $\text{MoO}_2$  affected negatively the ESA and ICR as well as the hydrophilic/hydrophobic properties of the PtCo/C catalyst. The addition,  $\text{TiO}_2$  at appropriate loading can enhance an increase of ESA as well as the decrease of ICR of the PtCo/C catalyst. Moreover, it can assist to manage the water in the catalyst layer. The PtCo/C catalyst with  $\text{TiO}_2$  of 0.06–0.15  $\text{mg/cm}^2$  can produce a maximum power density of 305  $\text{mW/cm}^2$  with a loss of around 20% of ESA after the repetitive potential cycling of 200 cycles.

## Acknowledgments

The authors would like to thank the Royal Golden Jubilee Ph.D. Program of the Thailand Research Fund (Grant No. PHD/0338/2552) and the Embassy of France in Thailand for financial support.

## References

- [1] Uribe-Godínez J, García-Montalvo V, Jiménez-Sandoval O. Development of Ir-based and Rh-based catalyst electrodes for PEM fuel cell applications. *Int J Hydrogen Energy* 2013;18:7680–3.
- [2] Little AD, Inc. Cost analysis of fuel cell system for transportation: baseline system cost estimate. Cambridge: Department of Energy Final Report; 2000 [cited October 19, 2015]. Available on-line: <[http://www.ott.doe.gov/pdfs/baseline\\_cost\\_model.pdf](http://www.ott.doe.gov/pdfs/baseline_cost_model.pdf)>.
- [3] Zhong H, Zhang H, Liang Y, Zhang J, Wang M, Wang X. A novel non-noble electrocatalyst for oxygen reduction in proton exchange membrane fuel cells. *J Power Sources* 2007;164(2):572–7.
- [4] Charretreux F, Jaouen F, Ruggeri S, Dodelet J. Fe/N/C nonprecious metal catalysts for PEM fuel cells: influence of the structural parameters of pristine commercial carbon blacks on their activity for oxygen reduction. *Electrochim Acta* 2008;53:2925–38.
- [5] Lefevre M, Proietti E, Jaouen F, Dodelet J-P. Iron-based catalysts with improved oxygen reduction activity in polymer electrolyte fuel cells. *Science* 2009;324:71–4.

- [6] Hernández-Hernández HM, Olivares-Ramírez JM, Jiménez-Sandoval O. Performance of novel bimetallic carbonyl clusters as PEM fuel cell anodes, a comparative study. *Int J Hydrogen Energy* 2013;38:7674–9.
- [7] Samaneh Sh, Jean H. Improved carbon nanostructures as a novel catalyst support in the cathode side of PEMFC: a critical review. *Carbon* 2015;94:705–28.
- [8] Samaneh Sh, Jean H. The effect of low platinum loading on the efficiency of PEMFC's electrocatalysts supported on TiO<sub>2</sub>-Nb, and SnO<sub>2</sub>-Nb: an experimental comparison between active and stable conditions. *Energy Convers Manage* 2015;103:681–90.
- [9] Bhlapibul S, Pruksathorn K, Piumsomboon P. The effect of the stabilizer on the properties of a synthetic Ni<sub>core</sub>-Pt<sub>shell</sub> catalyst for PEM fuel cells. *Renew Energy* 2012;41:262–6.
- [10] Calderón JC, Mahata N, Pereira MFR, Figueiredo JL, Fernandes VR, Rangel CM, et al. Pt-Ru catalysts supported on carbon xerogels for PEM fuel cells. *Int J Hydrogen Energy* 2012;37:7200–11.
- [11] Seifitokaldani A, Savadogo O. Electrochemically stable titanium oxy-nitride support for platinum electro-catalyst for PEM fuel cell applications. *Electrochim Acta* 2015;167:237–45.
- [12] Quan X, Mei Y, Xu H, Sun B, Zhang X. Optimization of Pt-Pd alloy catalyst and supporting materials for oxygen reduction in air-cathode microbial fuel cells. *Electrochim Acta* 2015;165:72–7.
- [13] Senevirathne K, Neburchilov V, Alzate V, Baker R, Neagu R, Zhang J, et al. Nb-doped TiO<sub>2</sub>/carbon composite supports synthesized by ultrasonic spray pyrolysis for proton exchange membrane (PEM) fuel cell catalysts. *J Power Sources* 2012;220:1–9.
- [14] Zamani P, Higgins D, Hassan F, Jiang G, Wu J, Abureden S, et al. Electrospun iron-polyaniline-polyacrylonitrile derived nanofibers as non-precious oxygen reduction reaction catalysts for PEM fuel cells. *Electrochim Acta* 2014;139:111–6.
- [15] Xu M, Li C, Ren H, Ding L, Xu K, Geng J. Carbon-supported Co-phthalocyanine modified with pyridine, 2-acid pyridine and 2-methyl pyridine as novel cathode catalysts for alkaline PEM fuel cells. *J Mol Cat A - Chem* 2014;390:69–75.
- [16] Bing Y, Liu H, Zhang L, Ghosh D, Zhang J. Nanostructured Pt-alloy electrocatalysts for PEM fuel cell oxygen reduction reaction. *Chem Soc Rev* 2010;39:2184–202.
- [17] Antolini E, Salgado JRC, Gozalez ER. The stability of Pt-M (M = first row transition metal) alloy catalysts and its effect on the activity in low temperature fuel cells: a literature review and tests on a Pt-Co catalyst. *J Power Sources* 2006;160:957–68.
- [18] Ohyagi Sh, Sasaki T. Durability of a PEMFC Pt-Co cathode catalyst layer during voltage cycling tests under supersaturated humidity conditions. *Electrochim Acta* 2013;102:336–41.
- [19] Yuan XZ, Li H, Zhang S, Martin J, Wang H. A review of polymer electrolyte membrane fuel cell durability test protocols. *J Power Sources* 2011;196:9107–16.
- [20] Avcioglu GS, Ficicilar B, Bayrakceken A, Eroglu I. High performance PEM fuel cell catalyst layers with hydrophobic channels. *Int J Hydrogen Energy* 2015;40:7720–31.
- [21] Blanco M, Wilkinson DP, Wang H. Application of water barrier layers in a proton exchange membrane fuel cell for improved water management at low humidity conditions. *Int J Hydrogen Energy* 2011;36:3635–48.
- [22] Wang Y, Wang L, Advani SG, Prasad AK. Double-layer gas diffusion media for improved water management in polymer electrolyte membrane fuel cells. *J Power Sources* 2015;292:39–48.
- [23] Kitahara T, Nakajima H, Okamura K. Gas diffusion layers coated with a microporous layer containing hydrophilic carbon nanotubes for performance enhancement of polymer electrolyte fuel cells under both low and high humidity conditions. *J Power Sources* 2015;283:115–24.
- [24] Chaisuban N, Pruksathorn K, Vergnes H, Hunsom M. Effect of the TiO<sub>2</sub> phase and loading on oxygen reduction reaction activity of PtCo/C catalysts in proton exchange membrane fuel cells. *Kor. J Chem Eng* 2015;32:1305–13.
- [25] Fugane K, Toshiyuki M, Ding RO, Suzuki A, Yoshikawa H, Masuda T, et al. Activity of oxygen reduction reaction on small amount of amorphous CeO<sub>x</sub> promoted Pt cathode for fuel cell application. *Electrochim Acta* 2011;56:3874–83.
- [26] Litster S, McLean G. PEM fuel cell electrodes: review. *J Power Source* 2004;130:61–76.
- [27] Rico-Pérez V, Bueno-López A. Effect of RhO<sub>x</sub>/CeO<sub>2</sub> calcination on metal-support interaction and catalytic activity for N<sub>2</sub>O decomposition. *Appl Sci* 2014;4:468–81.
- [28] Leelaruji L, Hunsom M. Alcohol reduction-mediated preparation of a nano-scale Pt/C electrocatalyst for the oxygen reduction reaction in PEM fuel cells. *Renew Energy* 2010;35:2422–30.
- [29] Pandolfo AG, Hollenkamp AF. Carbon properties and their role in supercapacitors. *J Power Sources* 2006;157:11–27.
- [30] Bracco G, Holst B, editors. *Surface science techniques, springer series in surface sciences*. Berlin, Heidelberg: Springer-Verlag; 2013.
- [31] Vuk AŠ, Boris Orel RJ, Draži G. The effect of surface hydroxyl groups on the adsorption properties of nanocrystalline TiO<sub>2</sub> films. In *J Photoenerg* 2005;7:163–8.
- [32] Kim HM, Seo SB, Kim DY, Bae K, Sohn SY. Enhanced hydrophilic property of TiO<sub>2</sub> thin film deposited on glass etched with O<sub>2</sub> plasma. *TEEM* 2013;14(3):152–5.
- [33] Buranawong A, Witit-anun N, Chaiyakun S. Total pressure and annealing temperature effects on structure and photo-induce hydrophilicity of reactive DC sputtered TiO<sub>2</sub> thin films. *Eng J* 2012;16:79–89.
- [34] Bard AJ, Faulkner LR. *Electrochemical methods: fundamentals and applications*. 2nd ed. New York: John Wiley & Sons; 2000.
- [35] Eppler AM, Ballard IM, Nelson J. Charge transport in porous nanocrystalline titanium dioxide. *Physica E* 2002;14:197–202.
- [36] Pomoni K, Sofianou MV, Georgakopoulos T, Boukos N, Trapalis C. Electrical conductivity studies of anatase TiO<sub>2</sub> with dominant highly reactive 001 facets. *J Alloys Comp* 2013;548:194–200.
- [37] Colón-Mercado HR, Kim H, Popov BN. Durability study of Pt<sub>3</sub>Ni<sub>1</sub> catalysts as cathode in PEM fuel cell. *Electrochem Commun* 2004;6:795–9.